THREE-DIMENSIONAL TOPOGRAPHIC MAPPING OF VERTICAL AND OVERHANGING SURFACES OF COASTAL CLIFFS USING UAV-BASED LIDAR DATASET

A Case Study in South Kuta District, Bali Island

(Pemetaan Topografi Tiga Dimensi Permukaan Vertikal dan Menggantung dari Tebing Pantai Menggunakan Data LiDAR Berbasis Wahana Tanpa Awak: Studi Kasus di Kecamatan Kuta Selatan, Pulau Bali)

Daniel Adi Nugroho
Master Program, Department of Geography,
Faculty of Mathematics and Natural Sciences, Indonesia University
St. Lingkar Kampus Raya, Pondok Cina, Beji, Depok, West Java, Indonesia 16424
E-mail: dnugroho@gmail.com

Diterima: 18 Februari 2021; Direvisi: 23 Mei 2021; Disetujui untuk Dipublikasikan: 24 Mei 2021

ABSTRACT

The availability of high-density LiDAR datasets, enabled by UAV-based airborne laser scanning, has allowed topographic mapping surveyors to see unprecedented details on the earth's surface. One of the problems faced in large-scale topographic mapping is generating proper three-dimensional contour lines for vertical cliffs, recesses, and overhangs, especially when the surface is covered by vegetation, which is quite common in the tropical area. This paper showcases the practical application of the LiDAR survey using an unmanned aerial vehicle and ground point classification process using the Simple Morphological Filter (SMRF) algorithm to produce high-fidelity, three-dimensional digital contour maps of coastal cliffs. By rotating the LiDAR dataset before the classification process to minimize overlapping surfaces, the entire dataset can be simulated as a 2.5-D surface. Therefore, the SMRF algorithm can be executed to classify all ground points on the cliff surface, including the overhangs and recesses. The resulting ground surface derived from this classification process provided a sufficient approximation of the real-world surface in overhanging cliffs and recesses while maintaining the conventional way to convey local landscape topography through three-dimensional contour lines.

Keywords: lidar, point cloud, simple morphological filter, ground classification, overhang, cliff modeling

ABSTRAK

Ketersediaan data LiDAR dengan kerapatan tinggi yang diperoleh dari pemindaian laser dari udara menggunakan wahana tanpa awak, telah memungkinkan surveyor *pemetaan topografi untuk melihat tingkat detail yang belum pernah terlihat sebelumnya di permukaan bumi. Salah satu masalah yang dihadapi dalam pemetaan topografi skala besar adalah pembuatan garis kontur tiga dimensi yang akurat untuk tebing vertikal, relung, dan permukaan menggantung, terutama ketika permukaan tersebut tertutup oleh vegetasi yang cukup umum terjadi di daerah tropis. Kajian ini akan menunjukkan aplikasi praktis dari* survey *LiDAR menggunakan wahana tanpa awak dan proses klasifikasi titik tanah menggunakan algoritma* Simple Morphological Filter (SMRF) *untuk menghasilkan peta kontur digital tiga dimensi dengan ketelitian tinggi dari tebing-tebing pantai. Dengan melakukan rotasi dataset LiDAR sebelum proses klasifikasi untuk untuk meminimalkan permukaan yang tumpang tindih, seluruh dataset dapat disimulasikan sebagai permukaan 2,5-D. Oleh karena itu, algoritma SMRF dapat dijalankan untuk mengklasifikasikan semua titik-titik tanah pada permukaan tebing, termasuk relung dan ceruk-ceruknya. Permukaan tanah yang dihasilkan oleh proses klasifikasi ini memberikan pendekatan yang cukup baik dari permukaan asli di tebing dan relung pantai sambil tetap mempertahankan pendekatan konvensional dalam penyajian topografi bentang alam lokal melalui garis kontur tiga dimensi.*

Kata Kunci: *lidar, data titik,* simple morphological filter, *klasifikasi tanah, menggantung, pemodelan tebing*

INTRODUCTION

The classification of bare earth surface from the laser point cloud is essential in the post-processing stage of topographic surveys using LiDAR technology. The level of detail captured by high-density LiDAR scanning enables planners and designers to understand better the work area's uniqueness, especially hard-to-reach terrain overgrown with vegetation. Recently, laser measurements through various techniques have been applied to obtain highly accurate Digital

Elevation Models of sea cliffs, which is very important in reconstructing the three-dimensional surfaces of near-vertical sea cliffs surfaces overlooking the sea (Ruberti et al, 2020). These physical models of the sea cliffs can be utilized to monitor landslide phenomena, characterize spatial discontinuity, and assess cliff stability by applying geomechanical models (Mancini et al., 2017). The precision monitoring of the coastal cliff is essential, especially when such sites are adjacent to buildings and infrastructures, since retreating coastal cliffs due to erosion from waves can be detrimental to such structures' stability. Very steep terrain and heavily vegetated cliffs are some of the factors that hinder the study of physical processes on shorelines, especially the acquisition of quantitative data (Hampton & Griggs, 2004).

Representing coastal cliff surfaces with acceptable accuracy is a challenge that needs to be overcome by scientists monitoring the coastal landforms (Xhardé et al., 2006) because vertical surfaces and recesses such as coastal cliffs, notches, and overhangs present a significant limitation to the completeness of the conventional airborne LiDAR survey in such areas. While a high-fidelity cliff surface can be generated from photogrammetric techniques (James & Robson, 2012), in some areas with vegetation overgrowth, the accuracy of such methods is limited since the surface modeled in photogrammetry is the topmost surface, which includes vegetation canopy, not the actual ground or the bare earth.

The advent of the off-the-shelf commercial-grade unmanned aerial vehicles (UAV) has revolutionized the geospatial industry as a whole, especially LiDAR topographic mapping. Coupled with the miniaturization of LiDAR scanners and precise positioning devices, UAVs can be used as a reliable vehicular platform to perform LiDAR surveys (Wallace et al., 2012). UAV-based LiDAR surveys have become a viable solution to survey areas that are too small or too dangerous to be surveyed using manned aircraft. One of the benefits of UAV-based LiDAR scanning is the capability to capture the point cloud of a cliff from the seaside, which will not be possible to be accomplished with a terrestrial laser scanner. Another advantage of the LiDAR survey using the UAV platform is the inherent versatility in flying much closer to the object of interest than conventionally-piloted aircraft platforms, hence increasing the details that can be captured through much higher point cloud density (Wallace et al., 2012).

A previous study by Pack et al., (2012) has shown that additional step can be done in TerraSolid software to achieve better point cloud classification results in such area by transforming surfaces that can only be represented in 3-D to surfaces that can be represented in 2.5-D space using a three-dimensional rotation of the LiDAR dataset.

This study aims to showcase the application of three-dimensional rotation of the LiDAR dataset to improve ground classification, and the final result will be produced as three-dimensional contour lines instead of a meshed surface. The accuracy of the contour lines should satisfy the requirements for 1:1,000 scale topographic mapping. The three-dimensional contour lines allow users to visualize and spatially analyze vertical cliffs and overhangs while retaining contour lines as one of the defining characteristics of a topographic map.

METHODS

Study Area

The LiDAR datasets used in this case study were taken from two distinct locations in the southern part of Bali Island, Indonesia, specifically in the Pecatu village in South Kuta District, as presented in **Figure 1**. The LiDAR data acquisition was undertaken in 2019 (site B) and 2020 (site A) by utilizing a survey-grade, UAV-based laser scanner. These two datasets show beach cliffs being studied, ranging from 30 meters to 150 meters high, with various vegetation coverage levels and canopy density.

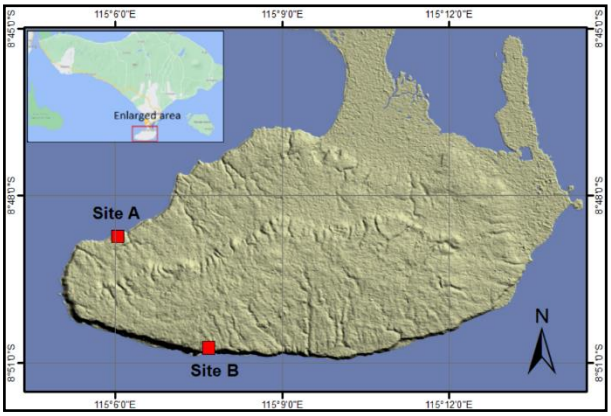

Figure 1. Study areas are located at the northern coast (site A) and southern coast (site B) of the Pecatu region, Bali. *Source: DEM Nasional (Badan Informasi Geospasial, 2020)*

These coastal cliffs at two opposite sides of the peninsula are part of the South Bali geological formation, consisting of partly bedded, recrystallized, and fossiliferous reef limestone (Purbo-Hadiwidjojo et al., 1998). Oblique aerial photos from the reconnaissance survey of the study areas are shown in **Figure 2** (Site A) and **Figure 3** (Site B).

The first dataset (from site A, located at 8° 48' 41" S, 115° 06' 02" E) contains a 30 meters tall, 430-meter wide cliff with a moderate degree of vegetation overgrowth, both on the top of the cliff and its midsection, and a significant amount of recesses and alcoves near to the sea surface. A large number of boulders scattered in the seawater

in front of a bare section of the cliff indicated that a portion of the cliff has detached from the main body due to marine erosion in relatively recent times. The second dataset (from site B, located at 8° 50′ 46″ S, 115° 07′ 39″ E) contains a 150-meter tall cliff, with a minimum amount of superficial vegetation cover and a wide but slender recess. Due to the limits imposed on private property access, the cliff face studied in the second dataset is narrower than the first dataset, at only 150 meters wide.

Figure 2. The 30-meter tall vegetated cliff face at Site A, with a significant amount of overhanging rock face and recesses.

Figure 3. The 150-meter tall, almost vertical cliff face at Site B, with slight recess at the lower part.

Control Network and Test Points

The base station coordinates for the LiDAR acquisition for both areas were surveyed using a CHC X900B GNSS receiver, referenced to station CDNP (located at 8° 49′ 05.18061″ S, 115° 08′ 44.35987″ E), which is part of Indonesia's Continuously Operating Reference Station (CORS) network. The ground test points were measured by employing a Real-Time Kinematic (RTK) GNSS survey technique.

LiDAR Data Acquisition

Since the cliffs are almost vertical and contain several overhangs, conventional methods of employing airborne LiDAR from manned aircraft and terrestrial laser scanner (TLS) is deemed unsuitable. Furthermore, the cost of the LiDAR survey using manned aircraft is deemed inefficient given the small size of the project area. A topographic survey using TLS is unsuitable due to the difficulty in covering the entire cliff surface, including its recesses and overhangs, from a safe observation point. The amount of vegetation overgrowth prevents cliff surface modeling through photogrammetry techniques. Therefore, a LiDAR survey from UAV platform is considered the best solution in this particular case.

Both LiDAR datasets were acquired using a Phoenix AL3-32 laser scanner equipped with KVH-1750 IMU and mounted on a DJI Matrice 600 UAV. For the GNSS base station, a CHC X900B GNSS receiver was used. The UAV was flown 50-60 meters in front of the rock-face at the seaside, running parallel to the coastline, to maximize the capture process of vertical surfaces on the coastal cliff. For Site B, multiple survey lines were made to cover the entire vertical distance of 150 meters from sea level to the top of the cliff. The kinematic GNSS survey method was employed in conjunction with IMU data to obtain the accurate flight trajectory of the UAV.

The ground coordinates of each point in the point cloud can be calculated by combining the information from the laser scanner, integrated GPS/INS navigation system, and the calibrated values of the laser scanner and its platform (Glennie, 2008). Such computation provides an unclassified point cloud as the basis for surface reconstruction and modeling. However, a ground classification process will need to be performed to ensure that the data points involved in the surface reconstruction actually represent the bare-earth surface. The established LiDAR georeferencing equation, according to Glennie (2008), is as follows **Formula 1**:

$$p_G^l = p_{GPS}^l + R_b^l(R_s^l r^s - l^b) \quad \text{.....(1)}$$

where p_G^l are the coordinates of the target point in the global reference frame, p_{GPS}^l are the coordinates of the GNSS sensor in the global reference frame, R_b^l is the rotation matrix from the navigation frame to the global reference frame, R_s^l is the rotation matrix from the scanner's frame to the navigation frame, r^s is the coordinates of the laser point in the scanner's frame, and l^b is the lever-arm offset between the scanner's initial origin and the navigation's origin. In order to georeference a single LiDAR return, all parameters must be determined for each laser pulse. Typically, the position, attitude, and motion of the scanning platform, which are sampled at a much lower rate than the laser scanner's pulse rate, are interpolated to line up with the LiDAR measurements. This set of information of positions and attitudes is then combined via **Formula 1** to create a georeferenced point cloud (Bell et al., 2020).

Classification of Ground Points

Classification of lidar point clouds to separate bare-earth from vegetation and other non-ground object is a crucial step in lidar mapping, and many lidar point filters have been developed for this purpose. Common bare-earth filters typically operate along a vector aligned with the LiDAR shot direction or referring to a vertical vector. These filters operate on a 2.5-D surface, which is suitable for creating 2.5-D products, such as digital elevation models and orthophotos (Pack et al., 2012). This 2.5-D space implies a planimetric position combined with a single value of height for each data point (Pfeifer, 2005), and most of the surface of the earth can be modeled in 2.5-D space.

Various studies on the ground-filtering algorithms, such as the study done by Zhang et al., (2003) on Progressive Morphological Filter (PMF) algorithm, (Zhang et al., 2016) on the Cloth Simulation Filter (CSF), and another study by Pingel et al., (2013) on the Simple Morphological Filter (SMRF) algorithm provides a viable open-source alternative to perform point cloud classification to established either commercial or proprietary software, such as TerraScan module in TerraSolid, LasGround tool in LASTools, and Auto Classify Ground Points tool in Global Mapper. These software packages can automatically distinguish ground points and non-ground points, in most cases. In reality, some areas on the earth's surface contain features that cannot be modeled satisfactorily in 2.5-D space, such as vertical cliffs and overhangs. When faced with such datasets, the ground classification algorithms in the aforementioned software packages will not produce realistic results since they will only look for the aerial low points and disregarding the overhanging surfaces. Valid bare-earth points that form the wall and the overhang surface will remain incorrectly classified as non-ground points.

As illustrated in **Figure 4**, the 2.5-D ground classification algorithms can be run directly for the first dataset (top) because only one possible Z-value can be inferred for each X-Y coordinates. In contrast, for the second dataset (bottom), there will be two Z-values for the overhanging part of the object, therefore typical ground class. To model vertical, near-vertical cliffs, and overhangs, additional steps need to be done to be classified appropriately by 2.5D classifiers. The automatic ground point classification tools integrated within leading LiDAR processing software suites such as Terrasolid, LASTools, PDAL, and CloudCompare works on 2.5-D space, in which only a single ground surface is considered within the classification algorithm.

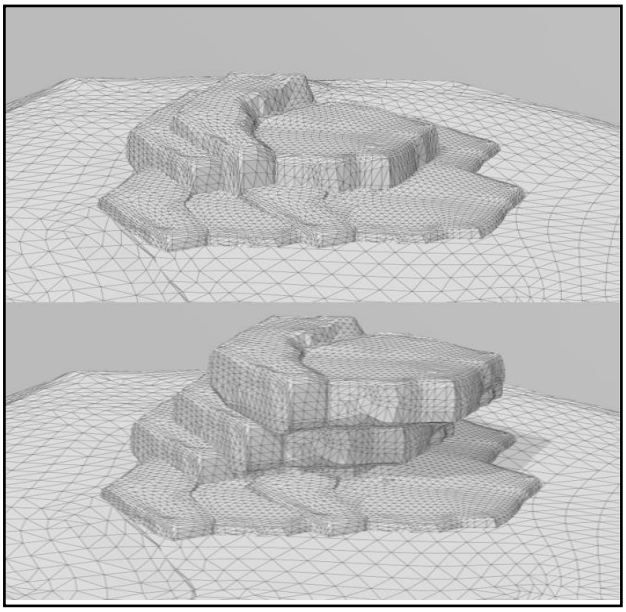

Figure 4. The object at the top can be modeled in 2.5-D, and the object at the bottom should be modeled in 3-D.

In this case study, the SMRF algorithm in the Point Data Abstraction Library (PDAL) software suite (Bell et al., 2020) is utilized. The SMRF algorithm consists of four conceptually distinct stages: 1) the creation of the minimum surface, 2) the processing of the minimum surface, in which grid cells from the raster are identified as either containing ground or non-ground points, 3) the creation of a DEM from these gridded points, and 4) the identification of the original LIDAR points as either bare earth or non-ground based on their relationship to the interpolated DEM (Pingel et al., 2013).

These stages are integrated into a single command in PDAL, with several parameters that can be set to adjust the algorithm's behavior. The SMRF algorithm is an improvement to the PMF algorithm, which was derived by K. Zhang et al. (2003) from a morphological filter originally proposed by Kilian et al. (1996), by gradually increasing the window size of the morphological filter to enable the filtering of all non-ground objects of various sizes.

First, the noises and outliers were removed from the LiDAR data by running the Noise Filter tool in CloudCompare. Only after all visible point data outliers from scanning artifacts are removed, subsequent processing can commence. Since the ground classification algorithm using the SMRF algorithm only works in 2.5-D space, a rotation of the dataset needs to be performed to enable the SMRF algorithm to classify bare ground on cliffs and overhangs, as illustrated in **Figure 6**. Rotation direction is determined by maximizing the surface of the cliff so that any overhanging surface is exposed towards the top view ground classifier algorithm works correctly. One of the simplest ways of determining the rotation is by fitting a planar surface to the LiDAR dataset block and then rotating

that planar surface to become completely horizontal.

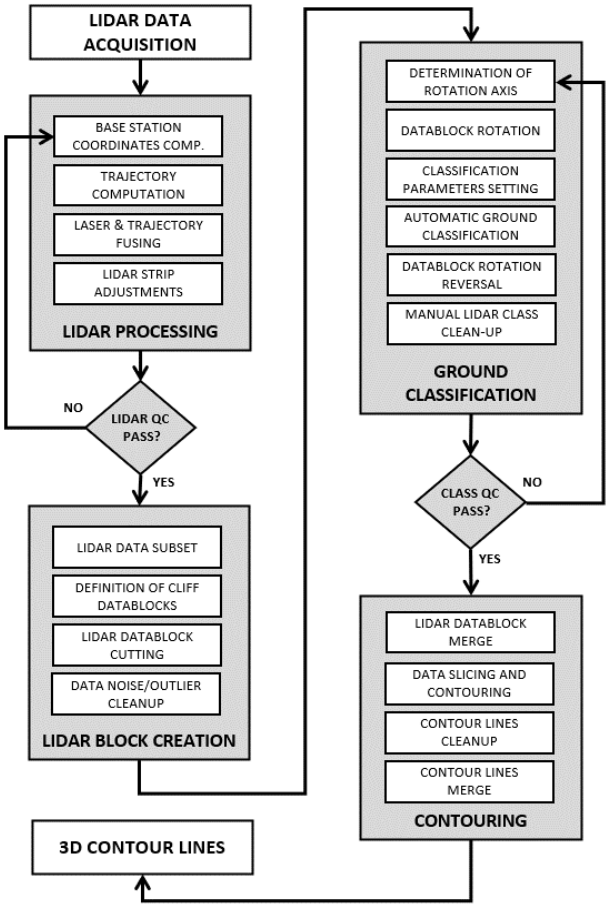

Figure 5. LiDAR data acquisition and processing workflow block diagram.

The Fit Plane tool in Cloud Compare software was used for each data block at the cliff area to obtain the rotation's magnitude and direction. The matrix that would make the fitted plane horizontal (normal towards Z+) can be found in the console area of CloudCompare after running the Fit Plane tool. The resulting rotation parameters were in the form of a 4x4 transformation matrix, which can be copied into the computer clipboard or exported into a text file for later use to restore the data block to its original position by using the inverse of the transformation matrix once the automated ground classification is completed. After the rotation parameters are determined by using the Fit Plane tool in CloudCompare, the subset of the LiDAR dataset can then be rotated with the center of the data segment as the point of origin. Using the Apply Transformation tool in CloudCompare, a transformation filter that applied an arbitrary rotation around a vector and represented as a 4x4 matrix to each XYZ triplet, blocks of LiDAR data can be rotated and ready to be processed further by the 2.5-D ground point classifier algorithm.

The 4x4 transformation matrix M can be expressed as a product of a rotation matrix R and translation matrix T, as shown in **Formula 2**.

$$M = \begin{bmatrix} R_{11} & R_{12} & R_{13} & 0 \\ R_{32} & R_{22} & R_{23} & 0 \\ R_{31} & R_{32} & R_{33} & 0 \\ 0 & 0 & 0 & 1 \end{bmatrix} \begin{bmatrix} 1 & 0 & 0 & T_x \\ 0 & 1 & 0 & T_y \\ 0 & 0 & 1 & T_z \\ 0 & 0 & 0 & 1 \end{bmatrix} \quad \text{.....(2)}$$

The rotated coordinates for each point within the point cloud can be calculated by using **Formula 3** as follows:

$$\begin{bmatrix} x_c \\ y_c \\ z_c \\ 1 \end{bmatrix} = M \begin{bmatrix} x \\ y \\ z \\ 1 \end{bmatrix} \quad \text{.....(3)}$$

where M is the transformation matrix; x_c, y_c, and z_c is the rotated coordinates of the point cloud; and x, y, z is the original coordinates. The elements of basic rotation matrix R around angle θ about an axis defined by a unit vector (*l,m,n*) can be expressed as the following set of equations (Szymanski, 1989):

$$R_{11} = ll(1-\cos\theta) + \cos\theta$$
$$R_{12} = ml(1-\cos\theta) - n\sin\theta$$
$$R_{13} = nl(1-\cos\theta) + m\sin\theta$$
$$R_{21} = lm(1-\cos\theta) + n\sin\theta$$
$$R_{22} = mm(1-\cos\theta) + \cos\theta$$
$$R_{23} = nm(1-\cos\theta) - l\sin\theta$$
$$R_{31} = ln(1-\cos\theta) - m\sin\theta$$
$$R_{32} = mn(1-\cos\theta) + l\sin\theta$$
$$R_{33} = nn(1-\cos\theta) + \cos\theta$$

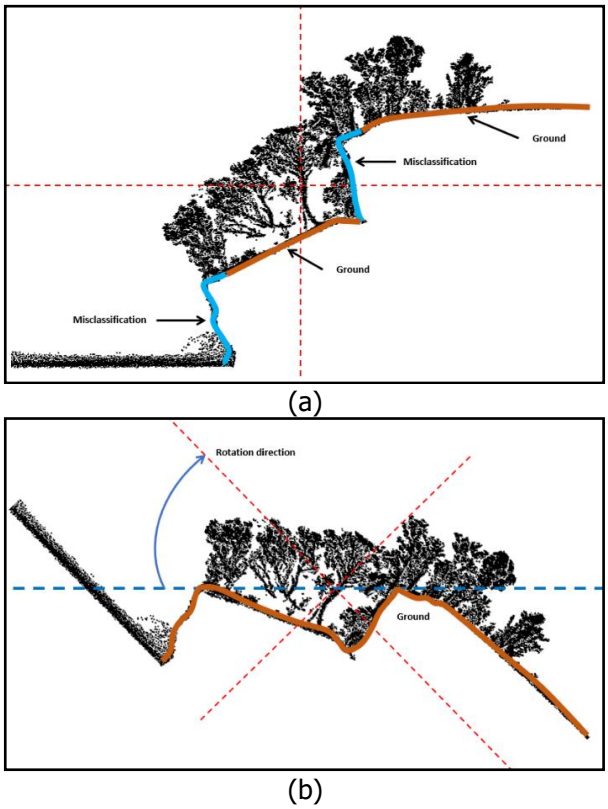

Figure 6. The original, unrotated dataset will have misclassified points due to overhanging parts (a); the rotated dataset will have correct ground classification since all overlapping terrain surfaces are eliminated temporarily during the classification process (b).

Rotating the whole LiDAR dataset for each study area may not be effective because 1) the variation of the terrain inclination over the entire width of the dataset was too much; consequently, the planar fitting algorithm will not reflect the inclination within localized surfaces, especially cliff surfaces; therefore, the resulting rotation matrix may not be sufficient to rotate the entire dataset and get proper 2.5-D space surface for all surfaces in the dataset; 2) large dataset will increase the requirement of free computer memory, the dense nature of LiDAR dataset collected using UAV tend to exhaust computer memory when the size is not appropriately managed. Hence, in most cases, it is necessary to compartmentalize the LiDAR dataset into smaller blocks to accommodate local terrain variation and to reduce computer memory requirement. These compartments or data blocks will be rotated individually to ensure every segment can be processed in 2.5-D space. The ground classification is done by employing the SMRF ground point filter in PDAL software suite (Bell et al., 2020) for each data segment. As soon as the automated ground point classification is completed in PDAL, an inverse rotation using the 4x4 transformation matrix that was saved previously will then performed to each data segment to return the LiDAR point cloud to its original position using Cloud Compare.

Point Classification Editing and Point Cloud Thinning

Based on visual inspection of the point cloud, it is apparent that the result of automated ground point cloud classification still contains artifacts or remnants of non-ground objects such as tree trunks or foliage, especially along the ridges and crests in the cliff surface. Manual intervention is needed by reclassifying such artifacts as noise points or other non-ground points. The manual reclassification was done by performing multiple visualizations of small cross-sections of a portion of the cliff to interpret ground and non-ground points and remove the artifacts manually. Professionally trained GIS data processing operators used the free Lasview module of the LASTools software (Isenburg, 2020) to perform this manual reclassification. Once the remaining artifacts were removed, a point-thinning algorithm was executed to get a thinned, uniform-density point cloud. The thinned point cloud will provide a more suitable surface for the contour line generation algorithm, which will help minimize the effort needed to edit the resulting contour lines manually. A voxel-based point-thinning algorithm in the PDAL software suite (voxel centroid-nearest neighbor) was used in this case study.

Three-dimensional Contour Line Generation

The Segmentation tool in CloudCompare software was used to generate contour lines with a specific interval. By employing the Slice function in the Segmentation tool followed by generation of the contour lines along with the horizontal slices, the outline of each horizontal cross-section of the LiDAR dataset can be produced, effectively creating the contour lines in three-dimension. The resulting contour lines were then manually edited to remove superfluous lines, to join fragmented contour lines, and to connect the contour lines of the cliff face to the contour lines of the inland topography. Contour lines in a digital three-dimensional topographic map will never cross each other since they will always be on different elevation levels from the reference datum. When viewed from the top, digital three-dimensional contour lines will appear similar to conventional paper-based topographic maps, where contour lines are not supposed to touch, overlap, or cross, except in certain rare instances such as if there is a vertical or overhanging cliff (Deline et al., 2015). In the case of a vertical cliff, the contour lines will appear to merge because they are right on top of each other when viewed from above, and in the case of an overhang, the contour lines will cross each other. The overall workflow of this case study is illustrated in **Figure 5**.

While the three-dimensional contour lines can convey the shape of the surface very well, *Portion de Ciel Visible* (PCV) algorithm, a point-and-mesh-shading algorithm which was based on an algorithm developed by Tarini et al., (2003), was used to provide a more compelling simulated visualization of the cliff surface. The PCV algorithm simulates the natural illumination of the scene as if there were spotlights sampled all over a hemisphere or a sphere, while the point cloud is lying at the center of this sphere, and this algorithm is available as one of the plug-ins in Cloud Compare software.

RESULTS AND DISCUSSION

In this case study, two sets of results were produced: 1) the three-dimensional contour lines as the primary product and 2) the PCV-shaded surface made by the ground point cloud to qualitatively gauge the completeness of the bare terrain representation in the classified data. The cliff face's visualization reconstructed using the ground points indicated that the cliff face, including the recesses, has been successfully preserved. A few deep alcoves were not scanned thoroughly by the LiDAR due to its location, but overall the cliff was reconstructed quite well, with almost no artifacts remaining. In Site A, some recessed areas at the bottom of the cliff near the ocean surface could not be adequately modeled due to inadequate LiDAR coverage in such a location.

LiDAR Accuracy Evaluation

A total of 140 ground test points were surveyed on both locations to provide reference data for the

accuracy evaluation in this case study. However, due to the inherent difficulty in measuring ground test points on the cliff wall, the test points were only placed on the cliff's top portion with a reasonable incline to ensure safe access by the surveying team. No test points were measured on the vertical wall and any overhanging surfaces. The root mean square error is used as a measure of LiDAR survey accuracy, which can be calculated based on **Formula 4** and **Formula 5** presented below:

$$RMSe_z = \sqrt{\sum_{i=1}^{n} \frac{(z_{laser} - z_{test})^2}{n}} \quad \text{.....(4)}$$

where $RMSe_z$ is the root mean square error, z_{laser} is the elevation of the terrain based on the laser ground points, z_{test} is the spot elevation of the terrain based on the terrestrial survey, and n is the number of observations. This formula can then be used to derive the linear error with 90% confidence (LE90) value by using the following equation (Badan Informasi Geospasial, 2014):

$$LE90 = 1.6499 \times RMSe_z \quad \text{.....(5)}$$

Based on the ground test points distributed on the bare area at the top side of the cliffs, vertical accuracy of 4.6 cm in RMSe was reported at site A, and vertical accuracy of 5.2 cm in RMSe was reported at site B, which translates to 6.9 cm of LE90 and 8.6 cm of LE90, respectively, according to **Formula 5**. This finding is on a par with the expected accuracy of the laser scanner (Phoenix LiDAR Systems, 2019) and well within the specification for a large-scale map in Indonesia on 1:1,000 scale maps, which limit the vertical error to 0.2 meter LE90, as defined by Indonesia's Geospatial Information Agency recent regulation on map accuracy standards (Badan Informasi Geospasial, 2014).

Only the vertical accuracy was evaluated in this case study. The horizontal accuracy was not evaluated due to the following factors: 1) no sufficient contrast provided by the laser intensity image to distinguish surficial features, 2) at the study area, there were no visibly identifiable angular features that can be detected in 3-D, such as building roofs, walls, and pavements edges, 3) time and budgeting constraints prevent the use of laser-reflective markers on ground test points to highlight their locations in the laser intensity image. Nevertheless, some of the ground test points were placed on top of the cliff ledges and the bottom of steep inclines to help point out any gross horizontal errors. In this case study, data from both areas do not show any gross horizontal positional errors.

Assessment of the Cliff Surface and Contour Lines

Visual examination of the contour lines produced by the CloudCompare segmentation tool shown no artifacts leftover from non-ground points due to vegetation and overgrowths. Note that some of the contour lines presented in **Figure 7** and **Figure 8** may appear to be overlapping with each other due to overhanging cliff faces. The contour lines flow naturally throughout the cliff and the overhangs, with a minimum amount of data gaps; however, the contour lines were fragmented and split in various locations, which requires a manual join using software to edit contour line shapefiles, in this case, QGIS (QGIS.org, 2020) was used, to improve the contour lines to adhere to cartographic standards.

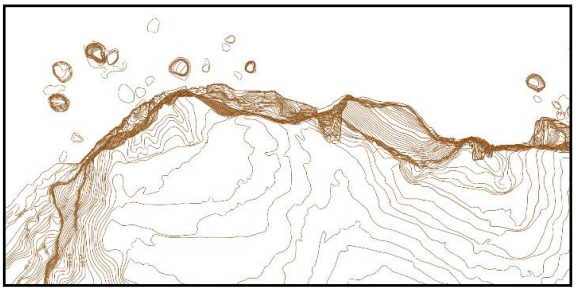

Figure 7. Contour lines of the cliff area at site A.

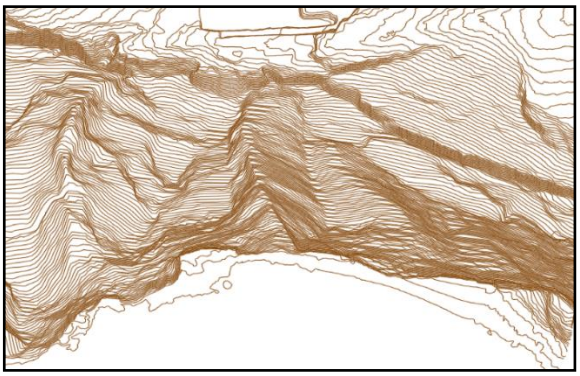

Figure 8. Contour lines of the cliff area at site B.

The edited contour lines of the cliff can then be joined with contour lines of the regular dataset from the main body of terrain to form a contiguous block of contour lines. Two sets of PCV-shaded visualization of the cliff area being studied were produced using CloudCompare software to assist in the qualitative assessment of the ground-filtering process. The oblique-angle visualization of the Site A is presented in **Figure 9**, and the visualization for Site B is presented in **Figure 10**. These visualizations can be rotated in CloudCompare to further examine the fidelity of the cliff surface reconstruction.

Employing the existing algorithm to classify ground points from the LiDAR dataset using the SMRF algorithm combined with the dataset's temporary rotation during algorithm execution has produced a satisfactory result. Manual efforts will still be needed to do the following steps: 1) orthogonally delineating approximate cliff face to derive segments used to rotate LiDAR points, 2) cleaning up the classified point cloud to remove artifacts from the automated classification

algorithm, and 3) editing and cleaning up the resulting contour lines to achieve acceptable standards in cartography.

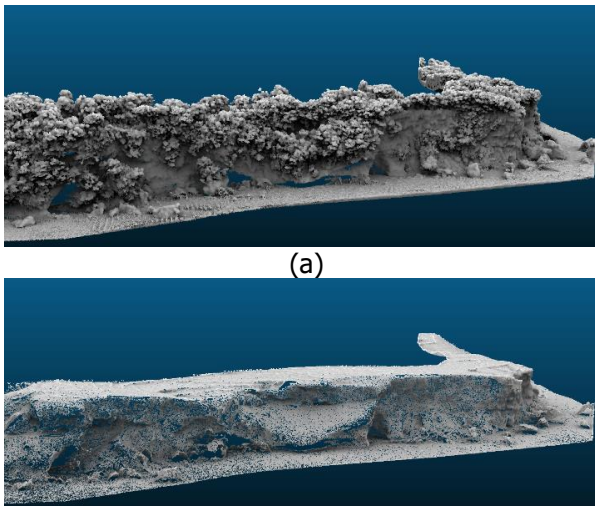

(a)

(b)

Figure 9. Perspective view of the raw, unclassified point cloud (a) compared to the classified ground point cloud (b) in site A.

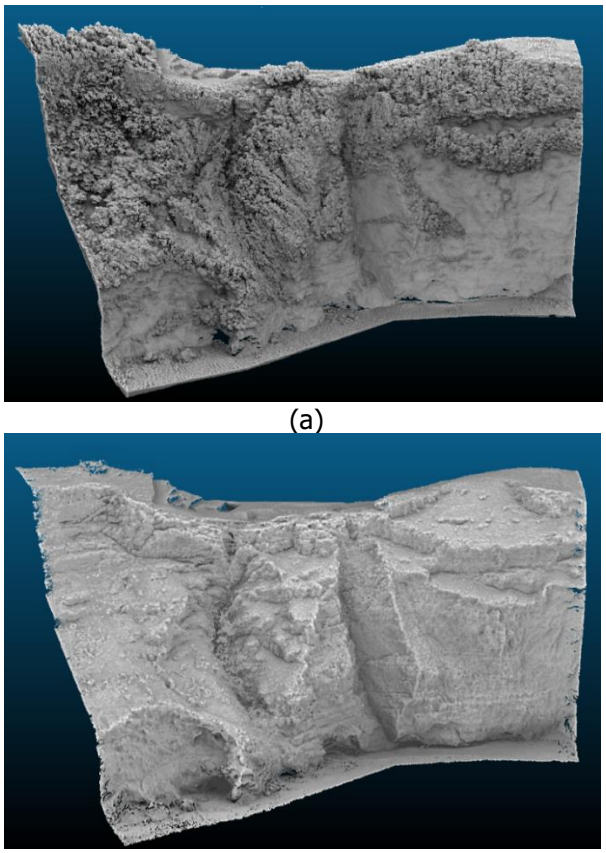

(a)

(b)

Figure 10. Perspective view of the raw, unclassified point cloud (a) compared to the classified ground point cloud (b) in site B.

The contour lines from the LiDAR dataset generated by slicing the point cloud in Z direction using CloudCompare software required a significant effort for cleaning up to meet cartographic standards. A more robust contouring tool that can generate more consistent contour lines from a particular point cloud class from the LiDAR dataset will reduce the person-hour involved.

In this case study, simple polygons were drawn manually along the approximated cliff face to split LiDAR dataset into smaller blocks, and then the rotation to an optimum horizontal plane for 2.5-D ground classification is done by performing a two-dimensional planar fitting to the LiDAR data block using CloudCompare. For smaller datasets like in this case study, such approximation is considered practical enough, but for larger datasets, a better procedural method in identifying rotation magnitude and direction in the form of 4x4 transformation matrices needs to be established.

Mapping the difficult-to-reach areas, such as the alcoves and deep recesses close to the sea surface, is proven to be problematic since the intrinsic risk associated with flying UAV close to the rough sea surface and the inability of the pilot to maintain a safe distance to the cliff face when no line of sight is possible. When no sufficient LiDAR data was acquired over such areas, manual interpretation has to be performed to be able to continue the contour lines crossing the area with data void. The small number of laser points in such locations was often get discarded in the noise-cleaning algorithm step. This predicament could be alleviated by employing a water-resistant UAV with a more advanced positioning system so that a more precise flight and a closer laser scanning to both the cliff and sea surface can be performed; hence more laser pulses can strike the surface of alcoves and recesses.

CONCLUSION

Airborne LiDAR survey using a UAV platform followed by data processing employing dataset rotation techniques prior to automatic ground point classification with SMRF algorithm has provided satisfactory results in capturing three-dimensional topographic maps of cliff surfaces in the Pecatu region in Bali. The cliff surfaces in both study areas were reconstructed successfully with sufficient accuracy for topographic mapping at 1:1,000 scale, and the final result can be presented in the form of three-dimensional contour lines.

ACKNOWLEDGMENTS

The LiDAR dataset for the two locations in this case study is provided through the courtesy of PT Tritara Orbit Surya, a topographic surveying and consulting company in Jakarta, Indonesia. The author is grateful to Dr. Parluhutan Manurung, PhD., from the Department of Geography, Faculty of Mathematics and Natural Sciences, Universitas Indonesia, for providing suggestions that resulted in substantial improvement of the manuscript.

REFERENCES

Badan Informasi Geospasial. (2014). Peraturan Kepala BIG Nomor 15 Tahun 2014 tentang Pedoman Teknis Ketelitian Peta Dasar. *Badan Informasi Geospasial. Bogor*.

Badan Informasi Geospasial. (2020). DEMNAS. Retrieved 27 May 2021, from https://tanahair.indonesia.go.id/demnas/#/#Info

Bell, A., Chambers, B., Butler, H., & Gerlek, M. (2020). *PDAL: Point cloud Data Abstraction Library Release 2.20*. Retrieved from https://pdal.io/PDAL.pdf

Deline, B., Harris, R., & Teffend, K. (2015). *Laboratory Manual for Introductory Geology* (Vol. 80). Dahlonega, Georgia: University of North Georgia Press. Retrieved from https://doi.org/10.2307/2482078

Glennie, C. (2008). Rigorous 3D error analysis of kinematic scanning LIDAR systems. *Journal of Applied Geodesy*, 1(3). Retrieved from https://doi.org/10.1515/jag.2007.017

Hampton, M. A., & Griggs, G. B. (2004). *Formation, Evolution, and Stability of Coastal Cliffs – Status and Trends*. *Professional Paper 1693*. Denver, Colorado: U.S. Geological Survey.

Isenburg, M. (2020). LASTools. https://rapidlasso.com/. Retrieved from http://rapidlasso.com/LAStools

James, M. R., & Robson, S. (2012). Straightforward reconstruction of 3D surfaces and topography with a camera: Accuracy and geoscience application. *Journal of Geophysical Research: Earth Surface*, 117(3), 1–18. Retrieved from https://doi.org/10.1029/2011JF002289

Kilian, J., Haala, N., & Englich, M. (1996). Capture and evaluation of airborne laser scanner data. *International Archives of Photogrammetry, Remote Sensing and Spatial Information Sciences*, 31, 383–388.

Mancini, F., Castagnetti, C., Rossi, P., Dubbini, M., Fazio, N. L., Perrotti, M., & Lollino, P. (2017). An integrated procedure to assess the stability of coastal rocky cliffs: From UAV close-range photogrammetry to geomechanical finite element modeling. *Remote Sensing*, 9(12), 1–22. Retrieved from https://doi.org/10.3390/rs9121235

Pack, R. T., Blonquist, K., & Carter, B. (2012). Lidar Bare-Earth Modeling Of Overhanging Cliffs-Extending 2.5-D Lidar Classifiers To Handle 3d Surface Classification Problems. In *ASPRS 2012 Annual Conference*. Sacramento, California.

Pfeifer, N. (2005). A subdivision algorithm for smooth 3D terrain models. *ISPRS Journal of Photogrammetry and Remote Sensing*. Retrieved from https://doi.org/10.1016/j.isprsjprs.2004.09.002

Phoenix LiDAR Systems. (2019). PLS AL3-32 Specification Sheet. Austin: Phoenix LiDAR Systems. Retrieved from www.phoenixlidar.com

Pingel, T. J., Clarke, K. C., & McBride, W. A. (2013). An improved simple morphological filter for the terrain classification of airborne LIDAR data. *ISPRS Journal of Photogrammetry and Remote Sensing*, 77(March), 21–30. Retrieved from https://doi.org/10.1016/j.isprsjprs.2012.12.002

Purbo-Hadiwidjojo, M., Samodra, H., & Amin, T. C. (1998). Systematic Geological Map of Indonesia. Bandung: Pusat Penelitian dan Pengembangan Geologi.

QGIS.org. (2020). QGIS Geographic Information System. Open Source Geospatial Foundation Project. Retrieved from http://qgis.org/

Ruberti, D., Marino, E., Pignalosa, A., Romano, P., & Vigliotti, M. (2020). Assessment of tuff sea cliff stability integrating geological surveys and remote sensing. Case history from Ventotene Island (Southern Italy). *Remote Sensing*, 12(12). Retrieved from https://doi.org/10.3390/rs12122006

Tarini, M., Cignoni, P., & Scopigno, R. (2003). Visibility based methods and assessment for detail-recovery. *Proceedings of the IEEE Visualization Conference*, 457–464. Retrieved from https://doi.org/10.1109/VISUAL.2003.1250407

Wallace, L. O., Lucieer, A., & Watson, C. S. (2012). Assessing the Feasibility of Uav-Based Lidar for High Resolution Forest Change Detection. *ISPRS - International Archives of the Photogrammetry, Remote Sensing and Spatial Information Sciences*, XXXIX-B7(September), 499–504. Retrieved from https://doi.org/10.5194/isprsarchives-xxxix-b7-499-2012

Xhardé, R., Long, B. F., & Forbes, D. L. (2006). Accuracy and limitations of airborne LiDAR surveys in coastal environments. *International Geoscience and Remote Sensing Symposium (IGARSS)*, 2412–2415. Retrieved from https://doi.org/10.1109/IGARSS.2006.625

Zhang, K., Chen, S. C., Whitman, D., Shyu, M. L., Yan, J., & Zhang, C. (2003). A progressive morphological filter for removing nonground measurements from airborne LIDAR data. *IEEE Transactions on Geoscience and Remote Sensing*, 41(4 PART I), 872–882. Retrieved from https://doi.org/10.1109/TGRS.2003.810682

Zhang, W., Qi, J., Wan, P., Wang, H., Xie, D., Wang, X., & Yan, G. (2016). An easy-to-use airborne LiDAR data filtering method based on cloth simulation. *Remote Sensing*, 8(6). Retrieved from https://doi.org/10.3390/rs8060501

Halaman ini sengaja kami kosongkan